Astronomy
&
Astrophysics

Accurate Ritz wavelengths of parity-forbidden [Fe II], [Ti II], and [Cr II] infrared lines of astrophysical interest⋆

M. Aldenius and S. Johansson

Atomic Astrophysics, Lund Observatory, Lund University, Box 43, 221 00 Lund, Sweden
e-mail: [maria;sveneric.johansson]@astro.lu.se

ABSTRACT

Context. With new astronomical infrared spectrographs the demands of accurate atomic data in the infrared have increased. In this region there is a large amount of parity-forbidden lines, which are of importance in diagnostics of low-density astrophysical plasmas.
Aims. We present improved, experimentally determined, energy levels for the lowest even LS terms of Fe II, Ti II and Cr II, along with accurate Ritz wavelengths for parity-forbidden transitions between and within these terms.
Methods. Spectra of Fe II, Ti II and Cr II have been produced in a hollow cathode discharge lamp and acquired using high-resolution Fourier Transform (FT) spectrometry. The energy levels have been determined by using observed allowed ultraviolet transitions connecting the even terms with upper odd terms. Ritz wavelengths of parity-forbidden lines have then been determined.
Results. Energy levels of the four lowest Fe II terms (a^6D, a^4F, a^4D and a^4P) have been determined, resulting in 97 different parity-forbidden transitions with wavelengths between 0.74 and 87 μm. For Ti II the energy levels of the two lowest terms (a^4F and b^4F) have been determined, resulting in 24 different parity-forbidden transitions with wavelengths between 8.9 and 130 μm. Also for Cr II the energy levels of the two lowest terms (a^6S and a^6D) have been determined, in this case resulting in 12 different parity-forbidden transitions with wavelengths between 0.80 and 140 μm.

Key words. atomic data – line: profiles – methods: laboratory – techniques: spectroscopic – infrared: general

1. Introduction

The interaction between laboratory and stellar spectroscopy has a long history, and still the availability of experimental atomic data is a necessity in analyses of stellar spectra. The development in astronomical instrumentation has also increased the demands on the accuracy of the data in the optical (e.g. the VLT/UVES spectrograph) and ultraviolet (e.g. the HST/STIS instrument) wavelength regions. The next step will be to improve the atomic database in the near-infrared region to match the needs defined by high-resolution spectra recorded with the newly installed CRIRES spectrograph at VLT and the space-borne SPITZER observatory.

The situation in nebular spectroscopy is quite different from the status of stellar spectroscopy. Nebular spectra show emission lines, and they are associated with various excitation mechanisms, general as well as selective. Very special features in nebular spectra are the "forbidden lines", i.e. transitions between metastable (long-lived) energy levels, which are only observable in spectra of very low-density plasmas. The forbidden lines are important for diagnostics of various parts of planetary nebulae (e.g. Smith et al. 2005) and nebular clouds around extended objects, such as active galactic nuclei, (see e.g. Kaufman et al. 2006; Meijerink et al. 2007). The diagnostics are often performed using standard pairs of forbidden lines, and the information embedded in numerous other forbidden lines is seldom exploited. This is partly due to the lack of reliable atomic data for forbidden lines.

Forbidden lines are not observed in light sources used for atomic spectroscopy, simply because collisions deexcite the

metastable levels due to the high electron density. The wavelengths can be calculated from the energy level values, but it is not until recently lifetime measurements of metastable levels in complex spectra have been performed using storage rings (Hartman et al. 2005). Astrophysical spectra have been used for converting the lifetimes into Einstein *A*-coefficients. Great efforts were early made by Garstang (e.g Garstang 1962) to calculate the *A*-coefficients, and they have later been followed up by work by Nussbaumer (Nussbaumer & Swings 1970; Nussbaumer & Storey 1988); Quinet (Quinet et al. 1996; Quinet 1997) and others. The theoretical data are certainly of high quality but they are not accompanied with any estimate of the uncertainty. However, accurate wavelengths can only be derived from experimental data.

In the present paper we present new and accurate wavelengths of forbidden lines in the infrared region for three spectra, Fe II, Ti II and Cr II, of high astrophysical relevance. Many of these lines have already been identified in astrophysical spectra, see e.g. Temim et al. (2006), Riffel et al. (2006), Hartman et al. (2004). Other second spectra of the iron group elements produce few forbidden lines in the infrared either because of the atomic structure or the low abundance. The energy level values of the lowest terms in Fe II, Ti II and Cr II have been improved by using observed UV-visible transitions measured with high-resolution Fourier Transform spectrometry. Accurate Ritz wavelengths have been determined for parity-forbidden transitions between and within these terms.

2. Experimental method

Spectra of Fe II, Ti II and Cr II were produced in a water cooled hollow cathode discharge lamp (HCL). Four different cathode

---

⋆ Tables 6–8 are only available in electronic form at
`http://www.aanda.org`

Table 1. Lamp conditions, spectrometer resolution and correction factors for the spectral acquisitions.

Spectrum number	Wavenumber range (cm^{-1})	Cathode material	Inserted metals	Carrier gas	Pressure (torr)	Current (mA)	Resolution (cm^{-1})	Calibration factor k_{eff}
I	22 200–44 200	Ti		Ar	0.6	500	0.05	$(1.43 \pm 0.02) \times 10^{-6}$
II	19 800–39 400	Fe		Ar	0.8	700	0.05	$(-2.34 \pm 0.02) \times 10^{-6}$
III	26 900–53 700	Fe		Ar	1.0	700	0.04	$(-2.54 \pm 0.03) \times 10^{-6}$
IV	21 700–43 400	Fe		Ne	1.2	1200	0.06	$(-2.90 \pm 0.03) \times 10^{-6}$
V	21 700–43 400	Fe		Ne	1.0	900	0.06	$(-2.90 \pm 0.03) \times 10^{-6}$
VI	20 600–41 000	Fe	Mg, Ti, Cr, Mn, Zn	Ar & Ne	0.9	700	0.05	$(-2.12 \pm 0.02) \cdot 10^{-6}$
VII	25 300–50 500	Fe	Mg, Ti, Cr, Mn, Zn	Ar & Ne	1.0	600	0.06	$(-2.23 \pm 0.03) \cdot 10^{-6}$
VIII	26 900–53 700	Fe	Mg, Cr, Zn	Ne	0.8	400	0.06	$(-3.19 \pm 0.04) \times 10^{-6}$
IX	26 900–53 700	Fe	Mg, Cr, Zn	Ne	0.9	500	0.06	$(-3.13 \pm 0.04) \times 10^{-6}$

compositions were used, see Table 1. In one spectral acquisition the cathode consisted of pure titanium, spectrum I, and for the others a cathode of pure iron was used. The cathodes had a cylindrical bore with an inner diameter of 6–7 mm and a length of about 50 mm. For four of the spectral acquisitions pieces of complementary metals were inserted in the cathode bore to produce spectra from several different ions simultaneously. Spectra II–IX were previously acquired for measurements of accurate relative wavelengths of different ions, see Aldenius et al. (2006). These spectra were complemented with spectrum I to improve the signal-to-noise ratios (*S/N*) and accuracy of the Ti II lines in this investigation. For the spectral acquisition with pure Ti or Fe cathodes argon or neon was used as a carrier gas, creating the initial plasma in the cathode. This provided Ar lines for wavelength calibration and Fe lines which were used as secondary calibration lines, see Sect. 3.1. For the spectral acquisitions with composite cathodes either a mixture of argon and neon or pure neon was chosen as the carrier gas. This was done because Ne produced higher *S/N* for lines that were too weak in pure Ar recordings. A continuous HCL mainly produces spectra from neutral and singly ionized species. To increase the amount of singly ionized species, and the *S/N* for the lines of interest, a large amount of spectra were recorded to achieve the best light source parameters. Finally, the light source was run with a current between 0.4 and 1.2 A and a pressure between 0.6 and 1.2 torr.

The spectra were acquired with the Chelsea Instruments FT500 UV Fourier Transform (FT) spectrometer (Thorne et al. 1987) in Lund. This is optimized to measure high-resolution spectra in the region 2000–7000 Å. Spectra for essentially two overlapping wavenumber regions, 20 000–40 000 cm^{-1} (5000–2500 Å), region A, and 26 000–50 000 cm^{-1} (3800–2000 Å), region B, were acquired using three different Hamamatsu photomultiplier tubes, R928 or 1P28 for region A and R166 for region B. Photon noise in the interferogram is transferred into the spectral region as white noise. All spectral lines seen by the detector contribute to this noise level. It is therefore an advantage to limit the light seen by the detector to the wavelength region of interest. The R166 detector used in region B is so-called solar-blind and has a long-wavelength cut-off at about 3000 Å. The short-wavelength cut-off for this region is at about 2000 Å, where air absorbs most light. For region A the R928 detector has a wide sensitivity range, between 2000 and 8000 Å, and an external 2 mm UG-5 optical glass filter was used to cut out light above 4000 Å, significantly reducing the noise. The two regions, including detectors and filter, overlap, giving a small region for transfer of calibration between them (see Sect. 3.1).

Table 2. Transition rules for allowed E1 and forbidden M1 and E2 transitions.

E1	M1	E2
Rules independent of coupling scheme		
parity change	no parity change	no parity change
$\Delta J = 0, \pm 1$	$\Delta J = 0, \pm 1$	$\Delta J = 0, \pm 1, \pm 2$
$(0 \leftrightarrow 0)$	$(0 \leftrightarrow 0)$	$(0 \leftrightarrow 0, \frac{1}{2} \leftrightarrow \frac{1}{2}, 0 \leftrightarrow 1)$

The light source was carefully aligned with a focusing lens at two different distances to the spectrometer. For spectra VII–IX (in region B) the light source was placed close to the aperture of the spectrometer, in order to decrease the light path length in air and thereby increase the *S/N* for the lines close to 2000 Å, where air absorbs most light. For the region at longer wavelengths (A) the light source was placed at a larger distance. In this wavelength region the absorption from air is less prominent. The resolution of the spectra was between 0.04 and 0.06 cm^{-1}, which was sufficient to completely resolve the lines. For each spectrum about 20 scans were co-added to achieve higher *S/N* for the lines. To further improve the accuracy the allowed E1 transitions were measured in several spectral recordings with different light-source parameters.

3. Analysis

For each of the three species the lowest LS terms of the low even configurations, including the ground term, were chosen to be included in the investigation. The upper levels of the parity-forbidden transitions should be meta-stable, having no level of opposite parity located at lower energy. It was also essential that the terms could be easily connected with UV-visible transitions through higher lying levels of opposite parity. To improve the accuracy of the lower levels, as many transitions to upper levels of odd parity as possible were chosen to be included in the measurements. Since the transition rules for allowed E1 transitions are $\Delta J = 0, \pm 1$, see Table 2, there was a maximum of three transitions to each upper level within one multiplet. To further improve the accuracy, lines were measured in at least three different spectral acquisitions.

Fe II has a complex energy level structure, with many low terms within a small energy interval. The ground state is 3d^6(^{5}D)4s a^{6}D$_{9/2}$ and the lowest terms belong to the even 3d^6(^{5}D)4s and 3d^7 configurations. The lower, even parity, energy levels of four different terms (a^{6}D, a^{4}F, a^{4}D and a^{4}P), with in total 16 energy levels between 0 and 13 900 cm^{-1}, were included in the investigation. Allowed UV-visible transitions to six terms of odd parity (z^{6}D, z^{6}F, z^{6}P, z^{4}F, z^{4}D and z^{4}P) were measured.
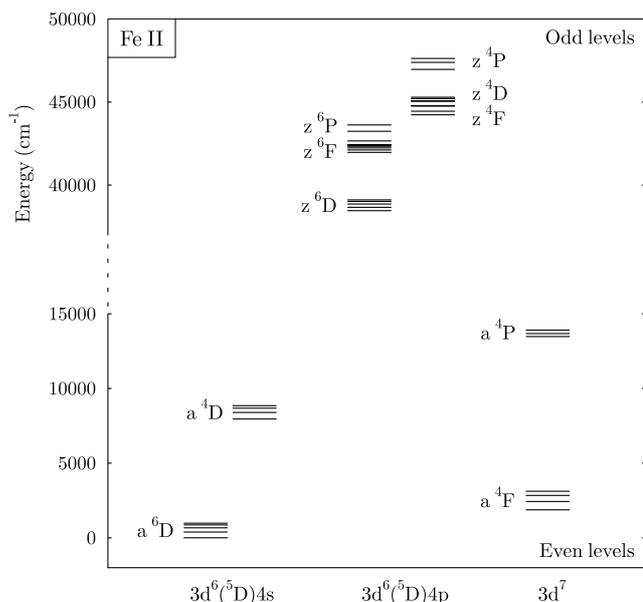
Fig. 1. Partial energy level diagram of Fe II displaying the low even levels and higher odd levels included in this investigation. Parity-forbidden M1 and E2 transitions occur between, and within, the even terms, while allowed E1 transitions between the odd and even terms are used for determining accurate energy level values.
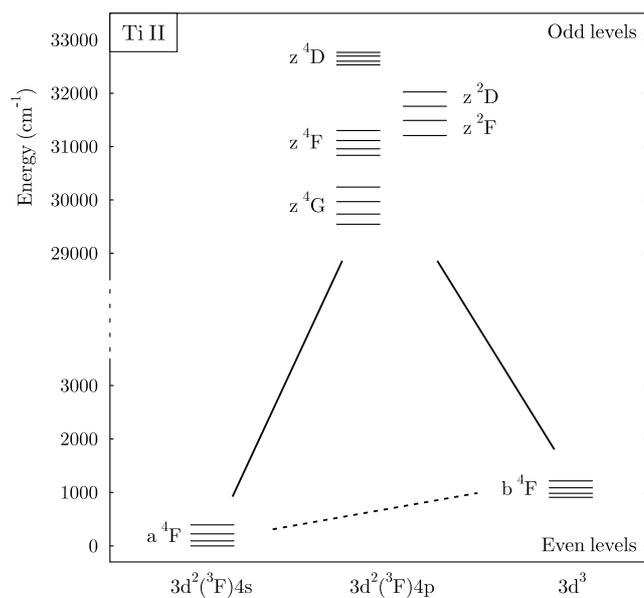

Fig. 2. Observed Fe II transitions, belonging to the a^4D–z^4P multiplet, from spectrum III. The wavelength span in the figure is about 6.6 Å and the weaker line at $39\,019\,cm^{-1}$ is an Ar II line from the carrier gas in the HCL.

These terms all belong to the $3d^6(^5D)4p$ configuration and are the lowest odd parity terms in Fe II with energies between $38\,000$ and $48\,000\,cm^{-1}$. A partial energy level diagram of Fe II is displayed in Fig. 1, including the even and odd terms considered in this investigation. Because of rather poor LS-coupling in Fe II, transitions between quartets and sextets have high probabilities and such intercombination lines were in general clearly visible in the laboratory spectra. This made it possible to connect the two spin systems. Figure 2 shows a small part of an observed spectrum (III) including three of the Fe II lines used in this investigation. The spectrum is from a pure iron cathode and contains iron and argon lines.

Also Ti II has a complex energy level structure with many low terms of even parity. The ground state is $3d^2(^3F)4s\ a^4F_{3/2}$ and the lowest terms belong to the $3d^2(^3F)4s$ and $3d^3$ configurations. The lower, even parity, energy levels of two different

Fig. 3. Partial energy level diagram of Ti II displaying the low even levels and higher odd levels included in this investigation. Parity-forbidden M1 and E2 transitions (dashed line) occur between, and within, the even terms, while allowed E1 transitions (solid lines) between the odd and even terms are used for determining accurate energy level values.
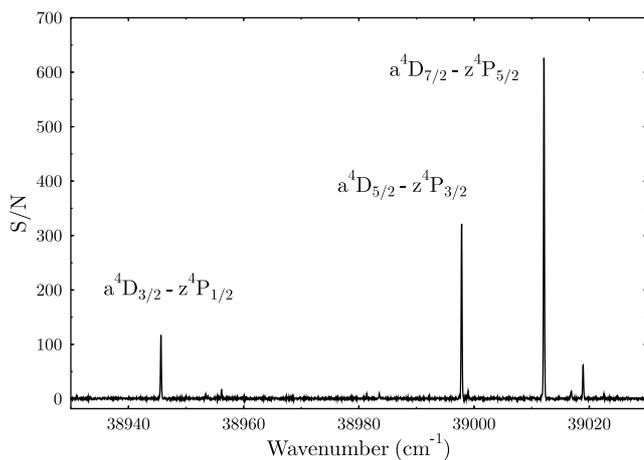
terms (a^4F and b^4F), with in total 8 energy levels between 0 and $1200\,cm^{-1}$, were included in the investigation. Allowed UV-visible transitions to five terms of odd parity (z^4G, z^4F, z^2F, z^2D and z^4D) were measured. These terms all belong to the $3d^2(^3F)4p$ configuration and are the lowest odd parity terms in Ti II with energies between $29\,000$ and $33\,000\,cm^{-1}$. A partial energy level diagram of Ti II including the even and odd terms in this investigation is shown in Fig. 3.

For Cr II the ground state is $3d^5\ a^6S_{5/2}$ and the lowest terms belong to the $3d^5$ and $3d^4(^5D)4s$ configurations. The lower, even parity, energy levels of two different terms (a^6S and a^6D), with in total 6 energy levels between 0 and $12\,500\,cm^{-1}$, were included in the investigation. The ground term has zero orbital angular momentum, $L = 0$, and therefore only one energy level ($J = \frac{5}{2}$). This means that the total number of possible transitions within, and between, these two lower terms are less than for e.g. Ti II. The lowest odd parity term in Cr II is z^6F at $47\,000\,cm^{-1}$, but transitions to the ground state from this term have very low transition probabilities (Nilsson et al. 2006). The second lowest odd term, z^6P, is at $48\,000\,cm^{-1}$, which results in transitions close to the $2000\,Å$ limit were air absorbs most light, making the observed transitions with low probabilities too weak. This made it possible to measure transitions only to (z^6P), belonging to the $3d^4(^5D)4p$ configuration. To try and compensate for this lack off useable transitions and improve the accuracies, the Cr II lines were measured in four different spectra.

3.1. Wavenumber calibration

FT spectrometry generates spectra with a linear wavenumber scale, whose accuracy derives from the control of the sampling of the interferogram by a single-mode helium-neon laser. The frequency of this control laser is stabilized to five parts in 10^9. The accuracy is, however, limited by the effects of using a finite-size aperture and by imperfect alignment of the light from the light source and the control laser (Learner & Thorne 1988).

To obtain a wavenumber scale, which is accurate to better than one part in 10^7, a multiplicative correction is applied, such that

$$\sigma_{corr} = (1 + k_{eff})\, \sigma_{obs} \qquad (1)$$

where σ_{corr} is the corrected wavenumber and σ_{obs} is the observed, uncorrected wavenumber. The correction factor, k_{eff}, is accurately determined by measuring the positions of well-known internal wavenumber standard lines. With FT spectra it is not necessary that the reference lines are evenly distributed throughout the spectrum. In principle, it is possible to use only one calibration line (Salit et al. 2004), but to reduce the uncertainty of the calibration, several calibration lines have been used for each spectrum. The use of internal calibration lines, in this case Ar II lines from the carrier gas in the HCL, helps to ensure, to as high degree as possible, that the light from the species being used for calibration illuminates the entrance aperture of the FT spectrometer in the same way as that of the species being investigated. Ar II lines are commonly used for wavelength calibration and there are in principle two sets of standard lines available. In this investigation wavenumbers from Whaling et al. (1995) have been used for calibration, rather than the work by Norlén (1973). For discussions on the difference between these two sets of lines see e.g. Whaling et al. (2002), Nave & Sansonetti (2004), Aldenius et al. (2006). The wavenumbers of Whaling were measured using FT spectrometry with molecular CO lines as wavenumber standards.

For spectral region A Ar II 4s-4p calibration lines with $S/N > 100$ were selected for the spectra with Ar as the carrier gas in the HCL (spectrum I, II and VI). Using only 4s-4p transitions decreases the risk of the lines being pressure shifted, since the pressure shift generally increases with excitation. 14 Ar II lines were used for each spectrum and the corresponding correction factor was derived by calculating the weighted mean of the 14 individual correction factors, where the weights were scaled with the inverse variance of each correction factor.

In spectral region B (spectrum III, VII, VIII and IX), covering higher wavenumbers, there are an insufficient number of reliable Ar II 4s-4p calibration lines available in our spectra. A transfer of calibration between the two spectral regions was therefore used. In spectrum VI, which includes the 14 Ar II calibration lines, a number of Fe I and Fe II lines were measured and calibrated. These lines are located in the overlap of the two spectral regions and are observed in all spectra containing iron. They could therefore be used, together with three Ar II lines when present, for calibration in region B. These Fe lines were also used for calibration in the spectra in region A with pure Ne as the carrier gas (spectrum IV and V). The uncertainty of the calibration in these spectra is slightly larger due to this two-step calibration, see Table 1.

3.2. Line profiles and blends

The observed lines were fitted with Voigt profiles using a least-square procedure included in the FT spectrometry analysis program XGREMLIN (Nave et al. 1997b), which is based on the GREMLIN code (Brault & Abrams 1989). This program was also used for transforming and phase correcting the measured interferograms. The fitted Voigt profiles showed low damping constants, implying that the observed lines were close to pure Gaussians. This was expected, since Doppler broadening is the dominant broadening effect in the HCL.

All lines, including calibration lines, had an apparently symmetric peak profile and showed no form of isotope or hyperfine structure. The metals all consisted of terrestrial relative abundances of the different isotopes. For Cr and Fe any isotope or hyperfine structure should be negligible compared to the Doppler width ($\sim$0.1–0.2 cm^{-1}) and they both have one dominating even isotope (^{52}Cr: 84% and ^{56}Fe: 92%). Ti consists of one even isotope with large relative abundance (^{48}Ti: 74%) and four other isotopes with relative abundances between 5 and 8%. Unresolved isotope structure itself should not pose a problem in wavenumber measurements, but if the observed lines are self-absorbed the different isotopes will be affected by varying amount of self-absorption and a small shift in the observed wavenumber could be introduced. If self-absorption was detected or suspected in a line this was investigated more thoroughly. By changing the discharge current in the HCL, and thereby producing different plasma densities, spectra were acquired with different amount of self-absorption. No tendency of wavenumber shift or asymmetric profiles were detected. All lines in the investigation were also measured in at least three different spectra with different plasma densities, and the possible effects should be negligible compared to the uncertainties from calibration and line fitting, see Sect. 4. Furthermore, all energy levels were derived by using several different transitions and observed lines which clearly gave different energy levels were removed from the fitting of energy levels, see Sect. 3.3.

All lines used in this work were carefully checked for possible blends from both the same species and other species present in the HCL. By using different HCL conditions with different carrier gas, cathode material and inserted metals the risk of not detecting unresolved blends was minimized.

Pressure shifts affect higher levels the most. In this investigation the highest levels included is at 48 000 cm^{-1}, which is relatively low. Nave et al. (1997a) estimated a shift of less than 0.005 cm^{-1} for levels at 100 000 cm^{-1} in Fe II when using a carrier gas pressure of at least 4 times higher than in this investigation. The spectra in this work were also tested for pressure shifts, see Aldenius et al. (2006), but no shifts were noted within 0.8 to 1.2 torr. In this investigation the difference in wavenumber between allowed transitions is used to determine the energy of the metastable levels and thus possible effects of pressure shifts on the higher odd levels become negligible.

3.3. Fitting of energy levels

For each species an energy level system was simultaneously fitted to all observed transitions, using a weighted least-square method. The weight of the wavenumber of an observed transition was based on the inverse variance and the ground state was considered fixed at zero energy with zero uncertainty. The procedure is described in detail in Öberg (2007) and is based on the method proposed by Radziemski et al. (1972). Ritz wavenumbers could then be derived from the fitted energy levels and the difference between these and the observed wavenumbers could be studied, see Fig. 4 for Fe II. Observed transitions which clearly deviated from the Ritz wavenumber ($|\sigma_{Ritz} - \sigma_{obs}| > 1.5 s_{obs}$) where investigated more thoroughly. If they showed any asymmetry in the observed profile or had a signal-to-noise ratio below 10 they were removed from the fitting procedure and the energy system was re-analyzed. This was done to avoid the influence from possible unknown unresolved blends, which could shift the wavenumber of the observed transition. Since all transitions were observed in several spectra, with different light source parameters, there were enough transitions to accurately determine the energy levels. For the cases of a transition being measured in several spectral acquisitions all of the observed wavenumbers
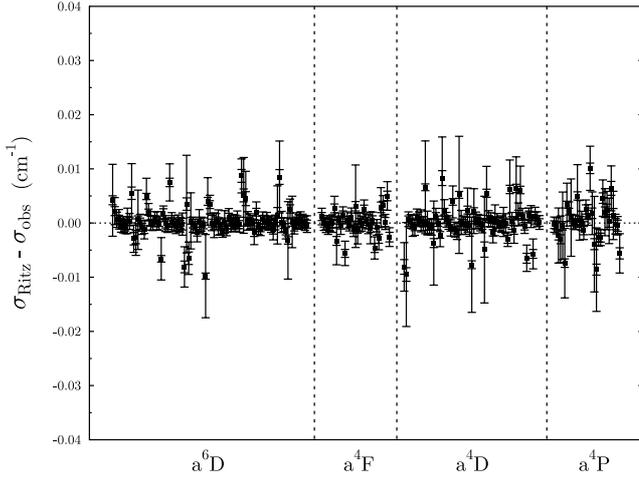
Fig. 4. The difference between calculated Ritz wavenumbers and observed wavenumbers for the observed UV Fe II lines. The x-axis is ordered in the four different lower terms and increases with the energy of the lower level and the observed wavenumber of the transition. The larger and smaller error bars represent the uncertainties in the observed wavenumbers and Ritz wavenumbers, respectively.

Table 3. Low lying Fe II energy levels of even parity.

Config.	Term	J	Energy (cm^{-1})	Unc. (cm^{-1})	Lines[a] (#)
3d^6(^{5}D)4s	a^{6}D	9/2	0	0	12[b]
		7/2	384.7868	0.0007	25
		5/2	667.6830	0.0008	27
		3/2	862.6108	0.0009	16
		1/2	977.0489	0.0010	13
3d^7	a^{4}F	9/2	1872.6005	0.0013	6
		7/2	2430.1369	0.0013	10
		5/2	2837.9803	0.0014	10
		3/2	3117.4889	0.0015	7
3d^6(^{5}D)4s	a^{4}D	7/2	7955.3189	0.0012	18
		5/2	8391.9562	0.0012	20
		3/2	8680.4708	0.0013	20
		1/2	8846.7822	0.0015	7
3d^7	a^{4}P	5/2	13 474.4487	0.0013	15
		3/2	13 673.2019	0.0014	10
		1/2	13 904.8598	0.0016	7

[a] Number of observed spectral features used in the determination of the energy. [b] Energy set to zero by definition.

were included in the fit of energy levels instead of first calculating a weighted mean.

For Fe II 96 different allowed transitions were used for determining the energy levels. The majority of the transitions were observed in at least two spectral recordings, and therefore in total 223 observed spectral lines, ranging from 31 000 to 44 400 cm^{-1}, were used in the analysis of Fe II. The transitions to the a^{4}P term have comparably low transition probabilities (see e.g. Kurucz & Bell 1995) and therefore appear as weak ($S/N \approx 5$–50), or not detectable, lines in the spectra acquired with Ar as the carrier gas in the HCL. To compensate for this recordings with pure Ne as the carrier gas were used, to increase the S/N of the observed lines. The values of the a^{4}P levels are therefore only slightly less accurate than the energies belonging to the lowest terms (a^{6}D, a^{4}F and a^{4}D). In Fig. 4 the difference between the calculated Ritz wavenumbers and the measured wavenumbers for the 223 observed lines is shown. The figure is divided into four parts
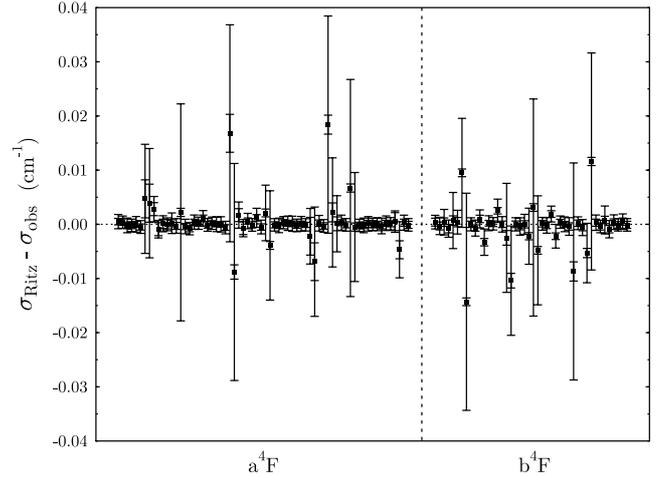

Fig. 5. The difference between calculated Ritz wavenumbers and observed wavenumbers for the observed UV-visible Ti II lines. See Fig. 4 for description of x-axis and error bars.

showing transitions to the four different lower terms. The transitions to the three lowest terms show mostly small error bars and are closely placed around zero difference, while the transitions to a^{4}P show a larger variance and a higher relative number of transitions with larger error bars. This is due to the weaker observed transitions to this term. The final values of the Fe II energy levels are presented in Table 3, together with the uncertainties and the number of observed spectral features used for determining each energy level.

For Ti II 65 different allowed transitions were used for determining the energy levels. The majority of these transitions were observed in at least two spectral recordings, and therefore in total 110 observed spectral lines, ranging from 28 500 to 39 600 cm^{-1}, were used in the analysis of Ti II. The two lowest terms in Ti II (a^{4}F and b^{4}F) are close in energy, within 1200 cm^{-1}, but they belong to different configurations (3d^2(^{3}F)4s and 3d^3 respectively). This means that the corresponding transitions to the two terms are close in wavenumbers and the intensity response in the spectra should be similar. Thus, the difference in observed line strength depend mainly on the difference in transition probabilities to the different terms. The transitions (within the stated wavenumber interval) to the ground term have in general higher branching fractions (and thus higher transition probabilities) (Pickering et al. 2001), but in most cases both kinds of transitions were clearly visible with high S/N (>100). This resulted in energy levels with similar uncertainties for both lower terms. In Fig. 5 the differences between the calculated Ritz wavenumbers and the observed wavenumbers for the 110 measured lines are shown. The figure is divided into two parts showing transitions to the two different lower terms. The transitions to both lower terms show mostly small error bars and are closely placed around zero difference. For the lowest term (a^{4}F) there are slightly more transitions and the relative number of observed wavenumbers with low uncertainty is also slightly higher. This difference has, however, a small impact on the uncertainties of the energy levels. The final values of the Ti II energy levels are presented in Table 4, together with the uncertainties and the number of observed spectral features used for determining each energy level.

For Cr II 12 different allowed transitions were used for determining the energy levels. The majority of these transitions were observed in at least two spectral recordings, and therefore in total 46 observed spectral lines, ranging from 36 100 to 48 600 cm^{-1}, were used in the analysis of Cr II. As discussed in the

Table 4. Low lying Ti II energy levels of even parity.

Config.	Term	J	Energy (cm^{-1})	Unc. (cm^{-1})	Lines[a] (#)
3d^2(^{3}F)4s	a^{4}F	3/2	0	0	15
		5/2	94.1105	0.0006	18
		7/2	225.7014	0.0007	19
		9/2	393.4442	0.0008	14
3d^3	b^{4}F	3/2	907.9646	0.0008	6
		5/2	983.9127	0.0006	16
		7/2	1087.3530	0.0007	13
		9/2	1215.8304	0.0009	9

[a] Number of observed spectral features used in the determination of the energy. [b] Energy set to zero by definition.

Fig. 6. The difference between calculated Ritz wavenumbers and observed wavenumbers for the observed UV-visible Cr II lines. See Fig. 4 for description of x-axis and error bars.

Table 5. Low lying Cr II energy levels of even parity.

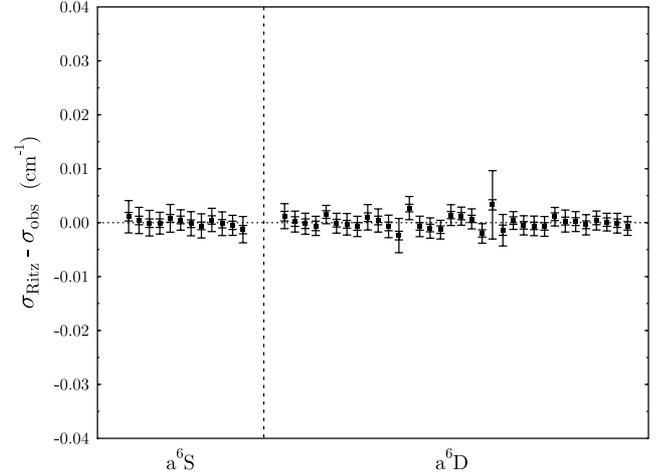| Config.	Term	J	Energy (cm^{-1})	Unc. (cm^{-1})	Lines[a] (#)
3d^5	a^{6}S	5/2	0	0	12[b]
3d^4(^{5}D)4s	a^{6}D	1/2	11 961.7452	0.0012	4
		3/2	12 032.5433	0.0009	8
		5/2	12 147.7694	0.0009	10
		7/2	12 303.8192	0.0008	8
		9/2	12 496.4549	0.0011	4

[a] Number of observed spectral features used in the determination of the energy. [b] Energy set to zero by definition.

introduction to Sect. 3 only transitions from one upper term was used for the determination of the energy levels of the two lowest terms in Cr II, but since four different acquired spectra were used the minimum number of observed lines used to determine an energy level was four. However, the uncertainties for the Cr II energy levels are somewhat higher than for most lower levels in Fe II and Ti II, due to the lack of transitions. In Fig. 6 the difference between the calculated Ritz wavenumbers and the observed wavenumbers for the 46 measured lines is shown. The figure is divided into two parts showing transitions to the two different lower terms. As the number of different transitions is much lower in this figure than in Figs. 4 and 5 the separate transitions can be distinguished. There is a clear pattern with groups of four observed lines (since four different spectra was used for most transitions). The decrease in $\sigma_{\text{Ritz}} - \sigma_{\text{obs}}$ within a group is evident and is a consequence to the way the x-axis is ordered (with increasing lower level and increasing observed wavenumber). It can also be noted that the scatter between the observed wavenumber, measured in different spectra, for the same transition is small and depend mostly on the wavenumber calibration of the different spectra. The final values of the Cr II energy levels are presented in Table 5, together with the uncertainties and the number of observed spectral features used for determining each energy level.

3.4. Ritz wavelengths

Ritz wavelengths are wavelengths derived from experimentally established energy levels. For Fe II, Ti II and Cr II the energy levels of the lowest even LS terms have been accurately determined in this work. Within and between these terms M1 and E2 transitions can occur following the transition rules in Table 2. For all possible M1 and E2 transitions the vacuum Ritz wavelength was calculated using the energy levels in Tables 3–5.

For Fe II this resulted in a total number of 97 different parity-forbidden transitions within a wavelength range of 0.74–87 μm. For most of these transitions the transition probability has been calculated by Quinet et al. (1996), who included only transitions for which A_{ki} was greater than 0.001 s^{-1}. In addition to these Quinet et al. (1996) also included transition probabilities for a couple of weaker infrared transitions for comparison with the values by Nussbaumer & Storey (1988). The published transition probabilities are the sum of both M1 and E2 transitions (if both contributed) and to be included the different types of radiation for a given transition had to be at least 1% of the sum of M1 and E2 contributions. Quinet et al. (1996) published both Superstructure and relativistic Hartree-Fock calculations for comparison, but states that the Superstructure

calculations should be more accurate. Therefore, we have chosen to only present these. The new Fe II Ritz wavelengths together with the transition probabilities and radiation types from Quinet et al. (1996) are presented in Table 6, sorted by multiplet.

For Ti II a total number of 24 different parity-forbidden transitions are presented. The wavelength range of the transitions is 8.9–130 μm. Unfortunately, to our knowledge, no transition probabilities for these transitions have been published. The new Ti II Ritz wavelengths are presented in Table 7, sorted by multiplet.

For Cr II a total number of 12 different parity-forbidden transitions, within a wavelength range of 0.80–140 μm, are presented. Calculated transition probabilities for the a^{6}S-a^{6}D transitions have been published by Quinet (1997), using a pseudo relativistic Hartree-Fock method. As for the Fe II transitions Quinet (1997) only included transitions for which A_{ki} was greater than 0.001 s^{-1}, and the published transition probabilities are the sum of both M1 and E2 transitions (if both contributed). The new Cr II Ritz wavelengths together with the transition probabilities and radiation types from Quinet (1997) are presented in Table 8, sorted by multiplet.

3.5. Wavelengths in air

Deriving the vacuum Ritz wavelengths from the experimentally determined energy levels is straight forward, since

$$\lambda_{\text{vac}} = 10^8 \times \frac{1}{\sigma}, \tag{2}$$

where λ_{vac} is in Å and σ is in cm^{-1}. The air wavelengths are, on the other hand, depending on the refractive index of air, n, so that

$$\lambda_{air} = 10^8 \times \frac{1}{n\sigma}. \tag{3}$$

The refractive index of air has been investigated at length (see e.g. Edlén 1966; Birch & Downs 1993; Ciddor 1996; Bönsch & Potulski 1998) and is accurately determined for the Visible to UV wavelength range, where the correction from vacuum to air is small. However for the infrared region the corrections become larger and the refractive index is not known to as good accuracy, due to the effects of water vapor and carbon dioxide. Ciddor (1996) focused on the visible to near infrared region, but states that the results agreed with the modified Edlén equations by Birch & Downs (1994). We have chosen to present the vacuum wavelengths together with air wavelengths derived by the Birch & Downs 1994 formula (based on the formula by Edlén 1966) for dry air (0.045% by volume of carbon dioxide) at 15°C and atmospheric pressure, as recommended by the CRC handbook of Chemistry & Physics (Lide 2006). Note however that the accuracy for wavelengths longer than $2\,\mu m$ is decreasing. The refractive index of air is depending on e.g. the temperature, pressure and humidity so for accurate use of air wavelengths the correct value should be calculated from the wavenumbers or the vacuum wavelengths.

4. Uncertainties

The Ritz wavelengths presented in this work are derived from experimentally determined energy levels, which in turn are determined by the measured wavenumbers of observed spectral lines. The uncertainties in the derived Ritz wavelengths for the M1 and E2 transitions depend thus on the uncertainties in the measured wavenumbers of the observed E1 transitions.

4.1. Observed wavenumbers

The uncertainties in the measured wavenumbers of the observed E1 transitions depend on both the uncertainty of the wavenumber calibration and on the uncertainty of the determination of the line position. The standard deviation $s(\sigma)$ of the line position σ of a fitted line profile can be written as (Brault 1987; Sikström et al. 2002)

$$s(\sigma) = \alpha_\sigma \frac{\sqrt{dx}}{S} \sqrt{w} = \alpha_\sigma \frac{w}{S \sqrt{n}}, \tag{4}$$

where S is the signal-to-noise ratio for the line, dx is the resolution interval and w is the FWHM of the line. The number of points across the width of the line is given by $n = w/dx$. α_σ is a numerical constant depending on the shape of the line, see Sikström et al. (2002).

The uncertainty from the calibration is derived from the uncertainties of the standard wavenumbers by Whaling et al. (1995) and from the uncertainties in the determinations of the line positions of the calibration lines in the spectra. With all possible systematic effects and uncertainties we used a conservative lower limit of 0.0010 cm^{-1} for the total uncertainties of the absolute wavenumbers of the observed lines, see e.g Learner & Thorne (1988).

The relative wavenumbers can be determined more accurately, since the uncertainty in the calibration and other systematic uncertainties have less significance, see

Aldenius et al. (2006). This leads to the fact that the energy levels, and Ritz wavelengths, can be more accurately determined than the observed wavenumbers.

4.2. Energy levels

The uncertainties in the fitted energy levels are given by the square root of the covariance in the fitting procedure, see Öberg (2007). In the least-square fitting routine an additional option of modifying the uncertainties of the observed wavenumbers is available. Two factors representing global corrections for underestimated uncertainties are included. This option was not used in this investigation, since the uncertainties of the observed wavenumbers were conservatively estimated and the calculated χ^2 values from the least-square fit were clearly smaller than the degrees of freedom of the system.

The uncertainties of the energy levels range from 0.0006 to 0.0016 cm^{-1}, where the lowest energies generally were determined more accurately due to the larger number of transitions connecting them to the ground state.

4.3. Ritz wavelengths

Ritz wavenumbers were calculated between energy levels included in the fit and the uncertainty for this wavenumber was given by the square root of the variance. The uncertainty of the corresponding vacuum wavelength is related to the uncertainty of the wavenumber as

$$\Delta\lambda_{vac} = 10^8 \times \frac{\Delta\sigma}{\sigma^2}, \tag{5}$$

and the wavelength uncertainties therefore increase for lower wavenumbers. The uncertainties in the Ritz wavenumbers range from 0.0005 to 0.0017 cm^{-1}, while the uncertainties in the vacuum wavelengths range from 0.00056 to 23 Å, depending greatly on the wavelength of the transition.

5. Results

For Fe II the experimentally determined energy levels are presented in Table 3 together with the estimated uncertainties. The energies range from 0 to 13 900 cm^{-1} and include the four lowest terms (a^{6}D, a^{4}F, a^{4}D and a^{4}P). The number of observed spectral lines used to determine each energy is also stated. Note that this number includes one or more observed lines of the same transition, since the spectral lines were in general observed in several of the acquired spectra. The derived Ritz wavenumbers, wavelengths and uncertainties for the parity-forbidden lines are presented in Table 6, together with calculated transition probabilities by Quinet et al. (1996). An extensive list containing wavelengths of parity-forbidden Fe II transitions has previously been published by Johansson (1977), who used a combination of grating spectroscopy and interferometric measurements. The study included wavelengths between 3000 and 12 000 Å and consisted of 281 parity-forbidden transitions. For lines included in both our work and the work of Johansson (1977), the uncertainties in our wavelengths are almost an order of magnitude lower.

For Ti II the energy levels are presented in Table 4 together with the estimated uncertainties. The energies range from 0 to 1200 cm^{-1} and include the two lowest terms (a^{4}F and b^{4}F). The derived Ritz wavenumbers, wavelengths and uncertainties for the parity-forbidden lines are presented in Table 7. No published

Table 9. Ritz wavelengths of prominent parity-forbidden lines of Ti II, Cr II and Fe II, sorted by wavelength. From Tables 6–8, which include the full set of lines with uncertainties and transition probabilities.

Ion	λ_{vac} (Å)	λ_{air} (Å)	Wavenumber (cm^{-1})	Multiplet
Fe II	7639.61670	7637.51419	13 089.6619	a^{6}D–a^{4}P
Fe II	7667.38923	7665.27922	13 042.2491	a^{6}D–a^{4}P
Fe II	7689.04345	7686.92760	13 005.5189	a^{6}D–a^{4}P
Cr II	8002.26949	8000.06908	12 496.4549	a^{6}S–a^{6}D
Cr II	8127.55768	8125.32343	12 303.8192	a^{6}S–a^{6}D
Cr II	8231.96395	8229.70150	12 147.7694	a^{6}S–a^{6}D
Cr II	8310.79498	8308.51122	12 032.5433	a^{6}S–a^{6}D
Cr II	8359.98415	8357.68710	11 961.7452	a^{6}S–a^{6}D
Fe II	8619.31631	8616.94915	11 601.8483	a^{4}F–a^{4}P
Fe II	8894.37171	8891.93015	11 243.0651	a^{4}F–a^{4}P
Fe II	9035.9708	9033.4909	11 066.8795	a^{4}F–a^{4}P
Fe II	9054.43465	9051.94977	11 044.3119	a^{4}F–a^{4}P
Fe II	9229.16055	9226.62838	10 835.2216	a^{4}F–a^{4}P
Fe II	9270.0992	9267.5560	10 787.3710	a^{4}F–a^{4}P
Fe II	9473.5428	9470.9444	10 555.7131	a^{4}F–a^{4}P
Fe II	12 570.2064	12 566.7681	7955.3189	a^{6}D–a^{4}D
Fe II	12 706.9109	12 703.4355	7869.7333	a^{6}D–a^{4}D
Fe II	12 791.2242	12 787.7260	7817.8600	a^{6}D–a^{4}D
Fe II	15 338.9391	15 334.7484	6519.3557	a^{4}F–a^{4}D
Fe II	15 999.1453	15 994.7751	6250.3339	a^{4}F–a^{4}D
Fe II	16 440.0180	16 435.5279	6082.7184	a^{4}F–a^{4}D
Fe II	16 642.2527	16 637.7076	6008.8019	a^{4}F–a^{4}D
Fe II	16 773.4034	16 768.8226	5961.8193	a^{4}F–a^{4}D
Fe II	17 454.1593	17 449.3933	5729.2934	a^{4}F–a^{4}D
Fe II	17 488.9900	17 484.2146	5717.8831	a^{4}D–a^{4}P
Fe II	17 975.9706	17 971.0627	5562.9820	a^{4}F–a^{4}D
Fe II	18 118.7982	18 113.8514	5519.1299	a^{4}D–a^{4}P
Fe II	18 139.2612	18 134.3089	5512.9037	a^{4}D–a^{4}P
Ti II	100 680.350	100 652.908	993.2425	a^{4}F–b^{4}F
Ti II	100 996.941	100 969.413	990.1290	a^{4}F–b^{4}F
Ti II	101 635.038	101 607.335	983.9127	a^{4}F–b^{4}F
Ti II	110 136.46	110 106.44	907.9646	a^{4}F–b^{4}F
Ti II	112 384.535	112 353.903	889.8021	a^{4}F–b^{4}F
Ti II	116 056.188	116 024.555	861.6516	a^{4}F–b^{4}F
Ti II	121 597.375	121 564.232	822.3862	a^{4}F–b^{4}F
Ti II	122 872.15	122 838.66	813.8540	a^{4}F–b^{4}F
Ti II	131 889.36	131 853.41	758.2113	a^{4}F–b^{4}F
Ti II	144 111.16	144 071.88	693.9088	a^{4}F–b^{4}F

experimental or calculated transition probabilities were available for these transitions.

For Cr II the energy levels are presented in Table 5 together with the estimated uncertainties. The energies range from 0 to 12 500 cm^{-1} and include the two lowest terms (a^{6}S and a^{6}D). The derived Ritz wavenumbers, wavelengths and uncertainties for the parity-forbidden lines are presented in Table 8, together with calculated transition probabilities by Quinet (1997).

The predicted strongest lines have been collected into a separate finding list arranged by wavelength in Table 9. These transitions have been chosen within the 0.76–15 μm region, which covers both the CRIRES region and part of the SPITZER region. Fe II and Cr II lines, which have calculated transition probabilities larger than 0.002 s^{-1} (Quinet et al. 1996; Quinet 1997) are included. Since no transition probabilities are available for the Ti II transitions we have chosen to include the a^{4}F–b^{4}F transitions with $\Delta J = 0, \pm 1$ in Table 9.

6. Conclusions

Data for forbidden lines in astrophysics are not easy accessible, in general, and for the infrared region, in particular. As forbidden lines by definition are associated with parity-forbidden transitions between low levels, many of the strongest lines appear in the near-infrared (transitions between LS-terms) and in the far-infrared (fine-structure transitions) in complex spectra. They are of great importance in nebular spectroscopy for studies of chemistry, temperature, density and dynamics of nebular clouds and regions.

To meet the requirements of accurate atomic data in the infrared region set by current and future high-resolution spectroscopy we have presented new wavelength measurements for forbidden lines of [Fe II], [Cr II] and [Fe II]. The data are based on revised energy level values obtained from very accurate wavelengths of allowed transitions in the three spectra studied.

References

Aldenius, M., Johansson, S., & Murphy, M. T. 2006, MNRAS, 370, 444
Birch, K. P., & Downs, M. J. 1993, Metrologia, 30, 155
Birch, K. P., & Downs, M. J. 1994, Metrologia, 31, 315
Bönsch, G., & Potulski, E. 1998, Metrologia, 35, 133
Brault, J. W. 1987, Mikrochim. Acta, 93, 215
Brault, J. W., & Abrams, M. C. 1989, High Resolution Fourier Transform Spectroscopy. OSA Technical Digest Series (Washington: Optical Society of America), 6, 110
Ciddor, P. E. 1996, Appl. Opt., 35, 1566
Edlén, B. 1966, Metrologia, 2, 71
Garstang, R. H. 1962, MNRAS, 124, 321
Hartman, H., Gull, T., Johansson, S., Smith, N., & HST Eta Carinae Treasury Project Team. 2004, A&A, 419, 215
Hartman, H., Johansson, S., Lundberg, H., et al. 2005, Phys. Scr. T, 119, 40
Johansson, S. 1977, Phys. Scr., 15, 183
Kaufman, M. J., Wolfire, M. G., & Hollenbach, D. J. 2006, ApJ, 644, 283
Kurucz, R., & Bell, B. 1995, Atomic Line Data (R.L. Kurucz and B. Bell) Kurucz CD-ROM No. 23. Cambridge, Mass.: Smithsonian Astrophysical Observatory, 1995., 23
Learner, R. C. M., & Thorne, A. P. 1988, J. Opt. Soc. Am. B, 5, 2045
Lide, D. R. 2006, CRC Handbook of chemistry and physics (CRC Handbook of chemistry and physics, 87th ed. by David R. Lide. Boca Raton: CRC Press, 2006)
Meijerink, R., Spaans, M., & Israel, F. P. 2007, A&A, 461, 793
Nave, G., & Sansonetti, C. J. 2004, J. Opt. Soc. Am. B, 21, 442
Nave, G., Johansson, S., & Thorne, A. P. 1997a, J. Opt. Soc. Am. B, 14, 1035
Nave, G., Sansonetti, C. J., & Griesmann, U. 1997b, in Fourier Transform Spectroscopy, OSA Technical Digest Series (Washington DC: Optical Society of America), 3, 38
Nilsson, H., Ljung, G., Lundberg, H., & Nielsen, K. E. 2006, A&A, 445, 1165
Norlén, G. 1973, Phys. Scr., 8, 249
Nussbaumer, H., & Storey, P. J. 1988, A&A, 193, 327
Nussbaumer, H., & Swings, J. P. 1970, ApJ, 162, 589
Öberg, K. J. 2007, Eur. Phys. J. D, 41, 25
Pickering, J. C., Thorne, A. P., & Perez, R. 2001, ApJS, 132, 403
Quinet, P. 1997, Phys. Scr., 55, 41
Quinet, P., Le Dourneuf, M., & Zeippen, C. J. 1996, A&AS, 120, 361
Radziemski, L. J., Fisher, K. J., Steinhaus, D. W., & Goldman, A. S. 1972, Comp. Phys. Commun., 3, 9
Riffel, R., Rodríguez-Ardila, A., & Pastoriza, M. G. 2006, A&A, 457, 61
Salit, M. L., Sansonetti, C. J., Veza, D., & Travis, J. C. 2004, J. Opt. Soc. Am. B, 21, 1543
Sikström, C. M., Nilsson, H., Litzén, U., Blom, A., & Lundberg, H. 2002, J. Quant. Spectr. Radiat. Transf., 74, 355
Smith, N., Balick, B., & Gehrz, R. D. 2005, AJ, 130, 853
Temim, T., Gehrz, R. D., Woodward, C. E., et al. 2006, ApJ, 132, 1610
Thorne, A. P., Harris, C. J., Wynne-Jones, I., Learner, R. C. M., & Cox, G. 1987, J. Phys. E, 20, 54
Whaling, W., Anderson, W. H. C., Carle, M. T., Brault, J. W., & Zarem, H. A. 1995, J. Quant. Spectrosc. Radiat. Transf., 53, 1
Whaling, W., Anderson, W. H. C., Carle, M. T., Brault, J. W., & Zarem, H. A. 2002, J. Res. NIST, 107, 149

Online Material

Table 6. Infrared Fe II Ritz wavelengths of parity-forbidden transitions. Sorted by multiplet.

Transition lower	Transition upper	Energy (cm^{-1})[a] lower	Energy (cm^{-1})[a] upper	Wavenumber (cm^{-1})	Unc. (cm^{-1})	λ_{vac} (Å)	Unc. (Å)	λ_{air}[b] (Å)	A_{ik}[c] (s^{-1})	Type
a^{6}D$_{9/2}$	a^{6}D$_{7/2}$	0	384	384.7868	0.0007	259 884.18	0.47	259 813.35	2.13×10^{-3}	M1
a^{6}D$_{9/2}$	a^{6}D$_{5/2}$	0	667	667.6830	0.0008	149 771.66	0.17	149 730.84		
a^{6}D$_{7/2}$	a^{6}D$_{5/2}$	384	667	282.8963	0.0005	353 486.48	0.66	353 390.13	1.57×10^{-3}	M1
a^{6}D$_{7/2}$	a^{6}D$_{3/2}$	384	862	477.8240	0.0007	209 282.08	0.31	209 225.04		
a^{6}D$_{5/2}$	a^{6}D$_{3/2}$	667	862	194.9277	0.0006	513 010.6	1.6	512 870.8	7.18×10^{-4}	M1
a^{6}D$_{5/2}$	a^{6}D$_{1/2}$	667	977	309.3658	0.0007	323 241.89	0.72	323 153.79		
a^{6}D$_{3/2}$	a^{6}D$_{1/2}$	862	977	114.4381	0.0006	873 834.8	4.9	873 596.7	1.89×10^{-4}	M1
a^{6}D$_{9/2}$	a^{4}F$_{9/2}$	0	1872	1872.6005	0.0013	53 401.674	0.036	53 387.117	9.15×10^{-5}	M1
a^{6}D$_{9/2}$	a^{4}F$_{7/2}$	0	2430	2430.1369	0.0013	41 149.946	0.021	41 138.726	3.04×10^{-5}	M1
a^{6}D$_{9/2}$	a^{4}F$_{5/2}$	0	2837	2837.9803	0.0014	35 236.326	0.017	35 226.718		
a^{6}D$_{7/2}$	a^{4}F$_{9/2}$	384	1872	1487.8137	0.0012	67 212.717	0.054	67 194.396	8.36×10^{-6}	M1
a^{6}D$_{7/2}$	a^{4}F$_{7/2}$	384	2430	2045.3501	0.0012	48 891.386	0.029	48 878.057	6.39×10^{-5}	M1
a^{6}D$_{7/2}$	a^{4}F$_{5/2}$	384	2837	2453.1935	0.0013	40 763.193	0.021	40 752.079	2.31×10^{-5}	M1
a^{6}D$_{7/2}$	a^{4}F$_{3/2}$	384	3117	2732.7020	0.0014	36 593.818	0.019	36 583.840		
a^{6}D$_{5/2}$	a^{4}F$_{9/2}$	667	1872	1204.9174	0.0012	82 993.239	0.085	82 970.617		
a^{6}D$_{5/2}$	a^{4}F$_{7/2}$	667	2430	1762.4538	0.0012	56 739.075	0.040	56 723.608	1.14×10^{-5}	M1
a^{6}D$_{5/2}$	a^{4}F$_{5/2}$	667	2837	2170.2973	0.0013	46 076.637	0.028	46 064.076	3.69×10^{-5}	M1
a^{6}D$_{5/2}$	a^{4}F$_{3/2}$	667	3117	2449.8058	0.0015	40 819.563	0.024	40 808.434	9.87×10^{-6}	M1
a^{6}D$_{3/2}$	a^{4}F$_{7/2}$	862	2430	1567.5261	0.0013	63 794.792	0.054	63 777.402		
a^{6}D$_{3/2}$	a^{4}F$_{5/2}$	862	2837	1975.3695	0.0014	50 623.440	0.036	50 609.639	8.89×10^{-6}	M1
a^{6}D$_{3/2}$	a^{4}F$_{3/2}$	862	3117	2254.8780	0.0015	44 348.297	0.030	44 336.206	1.51×10^{-5}	M1
a^{6}D$_{1/2}$	a^{4}F$_{5/2}$	977	2837	1860.9314	0.0015	53 736.531	0.042	53 721.883		
a^{6}D$_{1/2}$	a^{4}F$_{3/2}$	977	3117	2140.4399	0.0016	46 719.368	0.035	46 706.631	3.74×10^{-6}	M1
a^{6}D$_{9/2}$	a^{4}D$_{7/2}$	0	7955	7955.3189	0.0012	12 570.2064	0.0019	12 566.7681	4.74×10^{-3}	M1
a^{6}D$_{9/2}$	a^{4}D$_{5/2}$	0	8391	8391.9562	0.0012	11 916.1728	0.0018	11 912.9121	5.84×10^{-6}	E2
a^{6}D$_{7/2}$	a^{4}D$_{7/2}$	384	7955	7570.5321	0.0011	13 209.1112	0.0020	13 205.4994	1.31×10^{-3}	M1
a^{6}D$_{7/2}$	a^{4}D$_{5/2}$	384	8391	8007.1694	0.0012	12 488.8079	0.0018	12 485.3917	3.78×10^{-4}	M1
a^{6}D$_{7/2}$	a^{4}D$_{3/2}$	384	8680	8295.6840	0.0012	12 054.4611	0.0018	12 051.1629	2.62×10^{-6}	E2
a^{6}D$_{5/2}$	a^{4}D$_{7/2}$	667	7955	7287.6358	0.0012	13 721.8712	0.0022	13 718.1201	8.42×10^{-4}	M1
a^{6}D$_{5/2}$	a^{4}D$_{5/2}$	667	8391	7724.2731	0.0012	12 946.2020	0.0020	12 942.6616	1.98×10^{-3}	M1
a^{6}D$_{5/2}$	a^{4}D$_{3/2}$	667	8680	8012.7877	0.0013	12 480.0511	0.0020	12 476.6373	4.64×10^{-5}	M1
a^{6}D$_{5/2}$	a^{4}D$_{1/2}$	667	8846	8179.0992	0.0015	12 226.2853	0.0022	12 222.9404		
a^{6}D$_{3/2}$	a^{4}D$_{7/2}$	862	7955	7092.7081	0.0013	14 098.9871	0.0025	14 095.1335		
a^{6}D$_{3/2}$	a^{4}D$_{5/2}$	862	8391	7529.3454	0.0013	13 281.3671	0.0023	13 277.7357	1.17×10^{-3}	M1
a^{6}D$_{3/2}$	a^{4}D$_{3/2}$	862	8680	7817.8600	0.0014	12 791.2242	0.0022	12 787.7260	2.45×10^{-3}	M1
a^{6}D$_{3/2}$	a^{4}D$_{1/2}$	862	8846	7984.1714	0.0016	12 524.7812	0.0024	12 521.3552	6.46×10^{-4}	M1
a^{6}D$_{1/2}$	a^{4}D$_{5/2}$	977	8391	7414.9073	0.0014	13 486.3453	0.0025	13 482.6582		
a^{6}D$_{1/2}$	a^{4}D$_{3/2}$	977	8680	7703.4219	0.0014	12 981.2441	0.0024	12 977.6942	1.08×10^{-3}	M1
a^{6}D$_{1/2}$	a^{4}D$_{1/2}$	977	8846	7869.7333	0.0016	12 706.9109	0.0026	12 703.4355	3.32×10^{-3}	M1
a^{6}D$_{9/2}$	a^{4}P$_{5/2}$	0	13 474	13 474.4487	0.0013	7421.45 389	0.00072	7419.41 022		
a^{6}D$_{7/2}$	a^{4}P$_{5/2}$	384	13 474	13 089.6619	0.0012	7639.61 670	0.00073	7637.51 419	6.64×10^{-3}	M1
a^{6}D$_{7/2}$	a^{4}P$_{3/2}$	384	13 673	13 288.4152	0.0014	7525.35 188	0.00077	7523.28 019	9.25×10^{-5}	E2
a^{6}D$_{5/2}$	a^{4}P$_{5/2}$	667	13 474	12 806.7657	0.0013	7808.37 273	0.00078	7806.22 468	1.20×10^{-4}	M1, E2
a^{6}D$_{5/2}$	a^{4}P$_{3/2}$	667	13 673	13 005.5189	0.0014	7689.04 345	0.00083	7686.92 760	6.81×10^{-3}	M1
a^{6}D$_{5/2}$	a^{4}P$_{1/2}$	667	13 904	13 237.1768	0.0016	7554.48 095	0.00092	7552.40 140	2.03×10^{-4}	E2
a^{6}D$_{3/2}$	a^{4}P$_{5/2}$	862	13 474	12 611.8379	0.0014	7929.05 843	0.00086	7926.87 779	5.02×10^{-4}	M1
a^{6}D$_{3/2}$	a^{4}P$_{3/2}$	862	13 673	12 810.5912	0.0015	7806.04 101	0.00090	7803.89 359	3.76×10^{-4}	M1, E2
a^{6}D$_{3/2}$	a^{4}P$_{1/2}$	862	13 904	13 042.2491	0.0017	7667.38 923	0.00099	7665.27 922	6.23×10^{-3}	M1
a^{6}D$_{1/2}$	a^{4}P$_{5/2}$	977	13 474	12 497.3998	0.0014	8001.66 445	0.00091	7999.46 420	6.69×10^{-6}	E2
a^{6}D$_{1/2}$	a^{4}P$_{3/2}$	977	13 673	12 696.1531	0.0015	7876.40 158	0.00095	7874.23 516	9.80×10^{-4}	M1
a^{6}D$_{1/2}$	a^{4}P$_{1/2}$	977	13 904	12 927.8110	0.0017	7735.2616	0.0010	7733.1333	1.93×10^{-3}	M1

Table 6. continued.

Transition		Energy (cm⁻¹)[a]		Wavenumber	Unc.	λ_{vac}	Unc.	λ_{air}[b]	A_{ik}[c]	Type
lower	upper	lower	upper	(cm⁻¹)	(cm⁻¹)	(Å)	(Å)	(Å)	(s⁻¹)	
$a^4F_{9/2}$	$a^4F_{7/2}$	1872	2430	557.5364	0.0008	179 360.49	0.27	179 311.60	5.84×10^{-3}	M1
$a^4F_{9/2}$	$a^4F_{5/2}$	1872	2837	965.3798	0.0010	103 586.17	0.11	103 557.94		
$a^4F_{7/2}$	$a^4F_{5/2}$	2430	2837	407.8434	0.0009	245 192.12	0.52	245 125.29	3.92×10^{-3}	M1
$a^4F_{7/2}$	$a^4F_{3/2}$	2430	3117	687.3519	0.0011	145 485.88	0.23	145 446.22		
$a^4F_{5/2}$	$a^4F_{3/2}$	2837	3117	279.5085	0.0010	357 770.9	1.2	357 673.4	1.41×10^{-3}	M1
$a^4F_{9/2}$	$a^4D_{7/2}$	1872	7955	6082.7184	0.0007	16 440.0180	0.0020	16 435.5279	5.98×10^{-3}	E2
$a^4F_{9/2}$	$a^4D_{5/2}$	1872	8391	6519.3557	0.0008	15 338.9391	0.0019	15 334.7484	3.12×10^{-3}	E2
$a^4F_{7/2}$	$a^4D_{7/2}$	2430	7955	5525.1820	0.0007	18 098.9513	0.0023	18 094.0099	1.32×10^{-3}	E2
$a^4F_{7/2}$	$a^4D_{5/2}$	2430	8391	5961.8193	0.0007	16 773.4034	0.0020	16 768.8226	2.49×10^{-3}	E2
$a^4F_{7/2}$	$a^4D_{3/2}$	2430	8680	6250.3339	0.0008	15 999.1453	0.0020	15 994.7751	4.18×10^{-3}	E2
$a^4F_{5/2}$	$a^4D_{7/2}$	2837	7955	5117.3386	0.0009	19 541.4079	0.0033	19 536.0740	1.46×10^{-4}	E2
$a^4F_{5/2}$	$a^4D_{5/2}$	2837	8391	5553.9759	0.0008	18 005.1197	0.0025	18 000.2038	1.82×10^{-3}	E2
$a^4F_{5/2}$	$a^4D_{3/2}$	2837	8680	5842.4904	0.0007	17 115.9886	0.0022	17 111.3147	1.18×10^{-3}	E2
$a^4F_{5/2}$	$a^4D_{1/2}$	2837	8846	6008.8019	0.0010	16 642.2527	0.0027	16 637.7076	4.75×10^{-3}	E2
$a^4F_{3/2}$	$a^4D_{7/2}$	3117	7955	4837.8301	0.0011	20 670.4243	0.0045	20 664.7831		
$a^4F_{3/2}$	$a^4D_{5/2}$	3117	8391	5274.4674	0.0010	18 959.2603	0.0034	18 954.0849	2.98×10^{-4}	E2
$a^4F_{3/2}$	$a^4D_{3/2}$	3117	8680	5562.9820	0.0009	17 975.9706	0.0028	17 971.0627	2.12×10^{-3}	E2
$a^4F_{3/2}$	$a^4D_{1/2}$	3117	8846	5729.2934	0.0010	17 454.1593	0.0030	17 449.3933	2.47×10^{-3}	E2
$a^4F_{9/2}$	$a^4P_{5/2}$	1872	13 474	11 601.8483	0.0009	8619.31631	0.00067	8616.94915	3.56×10^{-2}	E2
$a^4F_{7/2}$	$a^4P_{5/2}$	2430	13 474	11 044.3119	0.0008	9054.43465	0.00068	9051.94 977	8.83×10^{-3}	M1, E2
$a^4F_{7/2}$	$a^4P_{3/2}$	2430	13 673	11 243.0651	0.0010	8894.37171	0.00076	8891.93 015	2.21×10^{-2}	E2
$a^4F_{5/2}$	$a^4P_{5/2}$	2837	13 474	10 636.4684	0.0009	9401.61678	0.00082	9399.03793	1.68×10^{-3}	M1, E2
$a^4F_{5/2}$	$a^4P_{3/2}$	2837	13 673	10 835.2216	0.0010	9229.16055	0.00088	9226.62 838	1.29×10^{-2}	E2
$a^4F_{5/2}$	$a^4P_{1/2}$	2837	13 904	11 066.8795	0.0013	9035.97077	0.0010	9033.4909	1.61×10^{-2}	E2
$a^4F_{3/2}$	$a^4P_{5/2}$	3117	13 474	10 356.9599	0.0011	9655.3429	0.0010	9652.6954	1.37×10^{-4}	E2
$a^4F_{3/2}$	$a^4P_{3/2}$	3117	13 673	10 555.7131	0.0012	9473.5428	0.0011	9470.9444	3.65×10^{-3}	E2
$a^4F_{3/2}$	$a^4P_{1/2}$	3117	13 904	10 787.3710	0.0014	9270.0992	0.0012	9267.5560	2.13×10^{-2}	E2
$a^4D_{7/2}$	$a^4D_{5/2}$	7955	8391	436.6373	0.0007	229 023.03	0.35	228 960.61	2.56×10^{-3}	M1
$a^4D_{7/2}$	$a^4D_{3/2}$	7955	8680	725.1519	0.0008	137 902.14	0.15	137 864.56		
$a^4D_{5/2}$	$a^4D_{3/2}$	8391	8680	288.5146	0.0007	346 602.93	0.79	346 508.46	1.36×10^{-3}	M1
$a^4D_{5/2}$	$a^4D_{1/2}$	8391	8846	454.8261	0.0010	219 864.27	0.48	219 804.35		
$a^4D_{3/2}$	$a^4D_{1/2}$	8680	8846	166.3115	0.0009	601 281.4	3.2	601 117.6	3.71×10^{-4}	M1
$a^4D_{7/2}$	$a^4P_{5/2}$	7955	13 474	5519.1299	0.0007	18 118.7982	0.0024	18 113.8514	2.23×10^{-3}	M1, E2
$a^4D_{7/2}$	$a^4P_{3/2}$	7955	13 673	5717.8831	0.0009	17 488.9900	0.0028	17 484.2146	2.25×10^{-3}	E2
$a^4D_{5/2}$	$a^4P_{5/2}$	8391	13 474	5082.4926	0.0007	19 675.3854	0.0028	19 670.0151	1.06×10^{-3}	M1, E2
$a^4D_{5/2}$	$a^4P_{3/2}$	8391	13 673	5281.2458	0.0009	18 934.9264	0.0032	18 929.7575	6.28×10^{-5}	M1, E2
$a^4D_{5/2}$	$a^4P_{1/2}$	8391	13 904	5512.9037	0.0012	18 139.2612	0.0038	18 134.3089	2.76×10^{-3}	E2
$a^4D_{3/2}$	$a^4P_{5/2}$	8680	13 474	4793.9780	0.0008	20 859.5034	0.0036	20 853.8108	3.67×10^{-4}	M1, E2
$a^4D_{3/2}$	$a^4P_{3/2}$	8680	13 673	4992.7312	0.0010	20 029.1176	0.0039	20 023.6509	6.35×10^{-4}	M1, E2
$a^4D_{3/2}$	$a^4P_{1/2}$	8680	13 904	5224.3891	0.0012	19 140.9940	0.0043	19 135.7690	9.09×10^{-4}	E2
$a^4D_{1/2}$	$a^4P_{5/2}$	8846	13 474	4627.6665	0.0011	21 609.1630	0.0052	21 603.2663	3.36×10^{-5}	E2
$a^4D_{1/2}$	$a^4P_{3/2}$	8846	13 673	4826.4197	0.0012	20 719.2921	0.0053	20 713.6376	5.77×10^{-4}	M1, E2
$a^4D_{1/2}$	$a^4P_{1/2}$	8846	13 904	5058.0776	0.0014	19 770.3569	0.0054	19 764.9607	4.04×10^{-5}	M1
$a^4P_{5/2}$	$a^4P_{3/2}$	13 474	13 673	198.7532	0.0010	503 136.5	2.4	502 999.4	1.86×10^{-4}	M1
$a^4P_{5/2}$	$a^4P_{1/2}$	13 474	13 904	430.4111	0.0012	232 336.01	0.67	232 272.68		
$a^4P_{3/2}$	$a^4P_{1/2}$	13 673	13 904	231.6579	0.0014	431 671.0	2.6	431 553.4	5.51×10^{-4}	M1

[a] Truncated energy. For more exact value see Table 3. [b] λ_{air} is calculated from the wavenumber using the modified Edlén (1966) dispersion formula by Birch & Downs (1994) for standard air. [c] Transition probabilities taken from the Superstructure calculations by Quinet et al. (1996).

Table 7. Infrared Ti II Ritz wavelengths of parity-forbidden transitions. Sorted by multiplet.

Transition lower	upper	Energy (cm^{-1})[a] lower	upper	Wavenumber (cm^{-1})	Unc. (cm^{-1})	λ_{vac} (Å)	Unc. (Å)	λ_{air} [b] (Å)
a^{4}F$_{3/2}$	a^{4}F$_{5/2}$	0	94	94.1105	0.0006	1 062 580.5	6.3	1 062 290.9
a^{4}F$_{3/2}$	a^{4}F$_{7/2}$	0	225	225.7014	0.0007	443 063.3	1.3	442 942.5
a^{4}F$_{5/2}$	a^{4}F$_{7/2}$	94	225	131.5909	0.0005	759 931.1	3.0	759 724.0
a^{4}F$_{5/2}$	a^{4}F$_{9/2}$	94	393	299.3337	0.0007	334 075.32	0.76	333 984.27
a^{4}F$_{7/2}$	a^{4}F$_{9/2}$	225	393	167.7428	0.0006	596 150.7	2.1	595 988.2
a^{4}F$_{3/2}$	b^{4}F$_{3/2}$	0	907	907.9646	0.0008	110 136.46	0.10	110 106.44
a^{4}F$_{3/2}$	b^{4}F$_{5/2}$	0	983	983.9127	0.0006	101 635.038	0.066	101 607.335
a^{4}F$_{3/2}$	b^{4}F$_{7/2}$	0	1087	1087.3530	0.0007	91 966.455	0.063	91 941.388
a^{4}F$_{5/2}$	b^{4}F$_{3/2}$	94	907	813.8540	0.0008	122 872.15	0.12	122 838.66
a^{4}F$_{5/2}$	b^{4}F$_{5/2}$	94	983	889.8021	0.0005	112 384.535	0.066	112 353.903
a^{4}F$_{5/2}$	b^{4}F$_{7/2}$	94	1087	993.2425	0.0006	100 680.350	0.061	100 652.908
a^{4}F$_{5/2}$	b^{4}F$_{9/2}$	94	1215	1121.7199	0.0008	89 148.817	0.062	89 124.518
a^{4}F$_{7/2}$	b^{4}F$_{3/2}$	225	907	682.2632	0.0009	146 571.01	0.19	146 531.06
a^{4}F$_{7/2}$	b^{4}F$_{5/2}$	225	983	758.2113	0.0006	131 889.36	0.10	131 853.41
a^{4}F$_{7/2}$	b^{4}F$_{7/2}$	225	1087	861.6516	0.0005	116 056.188	0.074	116 024.555
a^{4}F$_{7/2}$	b^{4}F$_{9/2}$	225	1215	990.1290	0.0007	100 996.941	0.072	100 969.413
a^{4}F$_{9/2}$	b^{4}F$_{5/2}$	393	983	590.4684	0.0007	169 357.06	0.21	169 310.90
a^{4}F$_{9/2}$	b^{4}F$_{7/2}$	393	1087	693.9088	0.0006	144 111.16	0.13	144 071.88
a^{4}F$_{9/2}$	b^{4}F$_{9/2}$	393	1215	822.3862	0.0006	121 597.375	0.087	121 564.232
b^{4}F$_{3/2}$	b^{4}F$_{5/2}$	907	983	75.9481	0.0009	1 31 6689.	15.	1 316 330.
b^{4}F$_{3/2}$	b^{4}F$_{7/2}$	907	1087	179.3884	0.0009	557 449.6	2.9	557 297.6
b^{4}F$_{5/2}$	b^{4}F$_{7/2}$	983	1087	103.4403	0.0007	966 740.9	6.2	966 477.4
b^{4}F$_{5/2}$	b^{4}F$_{9/2}$	983	1215	231.9177	0.0008	431 187.4	1.5	431 069.9
b^{4}F$_{7/2}$	b^{4}F$_{9/2}$	1087	1215	128.4774	0.0008	778 347.0	4.6	778 134.9

[a] Truncated energy. For more exact value see Table 4. [b] λ_{air} is calculated from the wavenumber using the modified Edlén (1966) dispersion formula by Birch & Downs (1994) for standard air.

Table 8. Infrared Cr II Ritz wavelengths of parity-forbidden transitions. Sorted by multiplet.

Transition lower	upper	Energy (cm^{-1})[a] lower	upper	Wavenumber (cm^{-1})	Unc. (cm^{-1})	λ_{vac} (Å)	Unc. (Å)	λ_{air} [b] (Å)	A_{ik} [c] (s^{-1})	Type
a^{6}S$_{5/2}$	a^{6}D$_{1/2}$	0	11 961	11 961.7452	0.0012	8359.98 415	0.00083	8357.68 710	8.40 × 10^{-2}	E2
a^{6}S$_{5/2}$	a^{6}D$_{3/2}$	0	12 032	12 032.5433	0.0009	8310.79 498	0.00065	8308.51 122	8.65 × 10^{-2}	E2
a^{6}S$_{5/2}$	a^{6}D$_{5/2}$	0	12 147	12 147.7694	0.0009	8231.96 395	0.00058	8229.70150	9.10 × 10^{-2}	E2
a^{6}S$_{5/2}$	a^{6}D$_{7/2}$	0	12 303	12 303.8192	0.0008	8127.55 768	0.00056	8125.32 343	9.76 × 10^{-2}	E2
a^{6}S$_{5/2}$	a^{6}D$_{9/2}$	0	12 496	12 496.4549	0.0011	8002.26 949	0.00071	8000.06908	1.06 × 10^{-1}	E2
a^{6}D$_{1/2}$	a^{6}D$_{3/2}$	11 961	12 032	70.7981	0.0011	1 412 467.	23.	1 412 083.		
a^{6}D$_{1/2}$	a^{6}D$_{5/2}$	11 961	12 147	186.0243	0.0011	537 564.3	3.3	537 417.8		
a^{6}D$_{3/2}$	a^{6}D$_{5/2}$	12 032	12 147	115.2262	0.0009	867 858.4	6.6	867 621.8		
a^{6}D$_{3/2}$	a^{6}D$_{7/2}$	12 032	12 303	271.2759	0.0010	368 628.4	1.4	368 527.9		
a^{6}D$_{5/2}$	a^{6}D$_{7/2}$	12 147	12 303	156.0497	0.0009	640 821.3	3.8	640 646.6		
a^{6}D$_{5/2}$	a^{6}D$_{9/2}$	12 147	12 496	348.6855	0.0012	286 791.4	1.0	286 713.2		
a^{6}D$_{7/2}$	a^{6}D$_{9/2}$	12 303	12 496	192.6358	0.0011	519 114.4	2.9	518 972.9		

[a] Truncated energy. For more exact value see Table 5. [b] λ_{air} is calculated from the wavenumber using the modified Edlén (1966) dispersion formula by Birch & Downs (1994) for standard air. [c] Transition probabilities taken from the calculations by Quinet (1997).